

Adapting a triple-axis spectrometer for small angle neutron scattering measurements

Mu-Ping Nieh,^{1(a)} Zahra Yamani,¹ Norbert Kučerka,¹ John Katsaras,¹ Darcy Burgess,² and Hugo Breton²

¹Canadian Neutron Beam Centre, Steacie Institute for Molecular Sciences, Chalk River Laboratory, National Research Council Canada, Ontario K0J 1J0, Canada

²Design and Fabrication Services, National Research Council Canada, 1200 Montreal Road, Ottawa, Ontario K1A 0R6, Canada

(Received 17 April 2008; accepted 21 July 2008; published online 5 September 2008)

Small angle neutron scattering (SANS) instruments typically cover a q (scattering vector) range from 0.001 to 0.6 \AA^{-1} . This range in q is achieved through a combination of cold neutrons ($\lambda > 4 \text{\AA}$) and a highly collimated beam. However, as a direct result of the unavailability of a cold source at the Canadian Neutron Beam Centre (CNBC), we have resorted to adapting a triple-axis spectrometer to perform SANS measurements. This is achieved through the use of multiple converging incident beams which enhance the neutron flux on the sample by a factor of 20, compared to a single beam of the same spot size. Furthermore, smearing effects due to vertical divergence from the slit geometry are reduced through the use of horizontal Soller collimators. As a result, this modified triple-axis spectrometer enables SANS measurements to a minimum q value (q_{\min}) of $\sim 0.006 \text{\AA}^{-1}$. Data obtained from the modified triple-axis spectrometer are in good agreement with those data from the 30 m NG3-SANS instrument located at the National Institute of Standards and Technology (Gaithersburg, MD, USA). © 2008 American Institute of Physics. [DOI: 10.1063/1.2969254]

I. INTRODUCTION

Small angle neutron scattering (SANS) has proven a powerful technique for the study of molecular structures and morphologies with length scales ranging from 10 to 1000 \AA . Dedicated SANS instruments normally cover a scattering vector range (q range) from 0.001 to 0.6 \AA^{-1} , where q is defined as $(4\pi/\lambda)\sin(\theta/2)$, and where λ and θ are the neutron wavelength and scattering angle, respectively. Measuring the lowest possible q value, q_{\min} , usually requires long wavelength neutrons and a small incident beam. Long wavelength neutrons are produced using cryogenic moderators (e.g., liquid hydrogen), shifting the thermal neutron energy distribution spectrum (Maxwellian) toward lower energies, while a small incident beam is generally produced using either a highly collimated, or focused,¹ neutron beam. In the case of a highly collimated beam, the reduced neutron flux on the sample is to some degree compensated by the use of a velocity selector, typically employed in SANS instruments, which increases the incident neutron bandwidth ($\Delta\lambda/\lambda$).

Presently, at the Canadian Neutron Beam Centre (CNBC) no cold source is available at the 120 MW National Research Universal (NRU) reactor. In order to adapt a triple-axis spectrometer for small angle measurements, the incident beam needs therefore to be highly collimated. Moreover, since a given incident neutron wavelength is selected through the use of a single crystal monochromator ($\Delta\lambda/\lambda$

$< 1\%$), instead of a velocity selector ($\Delta\lambda/\lambda \sim 10\%$), neutron flux incident on the sample is significantly reduced.

In a SANS experiment, the instrumental q resolution, $\Delta q/q$ (where Δq is the width of scattering vector distribution) is made up of two contributions:² (1) the angular resolution which is related to the collimation and (2) the wavelength resolution ($\Delta\lambda/\lambda$). In order to optimize neutron flux, the full width at half maximum full width at half maximum (FWHM) of λ is usually chosen to lie in the range between 10% and $\sim 30\%$ ($\Delta\lambda/\lambda$), making it comparable to the angular resolution.³ However, as mentioned, single crystal monochromators usually produce neutrons with a $\Delta\lambda/\lambda < 1\%$, dramatically reducing the incident neutron flux. Although there are ways to increase $\Delta\lambda/\lambda$, they usually involve a cost prohibitive redesign of the instrument.⁴⁻⁸

Another method of increasing incident neutron flux, while not increasing the beam size, is to employ multiple incident beams which converge at a single spot on the detector. This concept of one-dimensional confocal beams was first proposed and tested by Nunes⁹ and was further developed into two-dimensional (2D) confocal beams by Glinka, *et al.*¹⁰ At CNBC we have designed and implemented a confocal Soller collimator (CSC) for use at the N5 triple-axis spectrometer, making it suitable for SANS measurements. Compared to a single beam of given $\Delta\lambda/\lambda$ and dimension, at a q_{\min} of $\sim 0.006 \text{\AA}^{-1}$ the new CSC increases incident neutron flux at the sample by a factor of 20. This development allows for the ubiquitous triple-axis spectrometer to double, with little cost and effort, as a capable SANS instrument. Moreover, this design is different from the double crystal

^{a)}Tel.: 613-584-8811. FAX: 613-584-4040. Electronic mail: mu-ping.nieh@nrc.gc.ca.

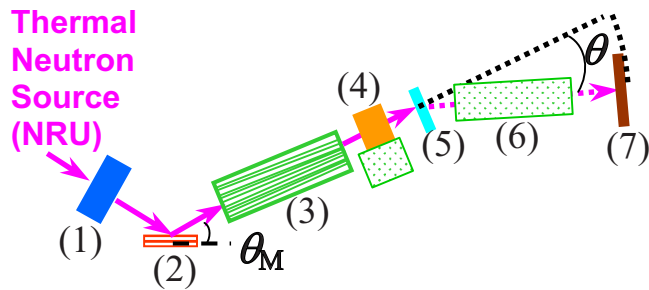


FIG. 1. (Color online) Schematic of the N5-SANS adapted from a triple-axis spectrometer to an instrument capable of SANS measurements. The components are as follows: (1) sapphire or Be filter. (2) Monochromator. (3) 23-channel CSC. (4) PG filter/21.6 cm long HSC/open. (5) Sample. (6) 48 cm long HSC. (7) 32-wire position sensitive detector.

diffraction technique developed by Bones and Hart.^{11–14} Due to the slit geometry of the incident beam, an additional horizontal Soller collimator (HSC) is required on the scattered side (detector) in order to reduce the smearing due to vertical divergence. However, in some cases the use of an HSC is also needed on the incident side. In order to validate our data, they were compared to those collected at the 30 m NG3-SANS instrument located at the National Institute of Standards and Technology (NIST). The comparison between the different data sets showed excellent agreement.

II. INSTRUMENT CONFIGURATION

Figure 1 shows a schematic of the N5 triple-axis spectrometer adapted for SANS measurements (N5-SANS). The source-to-monochromator distance, D_{SM} , is 6.78 m. However the neutrons are collimated at a distance of 0.91 m downstream from the source using an 8.9 cm(height) \times 5.9 cm(width) beam channel. This results in a new source-to-monochromator distance, D_{SM} , of 5.87 m.

In order to cover an extended q range, different λ 's are used. However, depending on the monochromator crystal planes used to select λ [e.g., pyrolytic graphite (PG) (002) reflection], the incident neutron beam can be contaminated by higher order harmonics of the fundamental neutron wavelength (i.e., $\lambda/2$, $\lambda/3$, etc.). In the current SANS experimental setup three values of λ (2.37, 4, and 5.23 Å) are used. Higher order harmonic neutrons are reduced either through the use of a beryllium (Be) ($\lambda > 3.99$ Å) or PG filter ($\lambda = 2.37$ Å). A sapphire filter is optionally used for reducing the presence of “fast neutrons.”¹⁵ Therefore, depending on the chosen wavelength, either a sapphire ($\lambda \leq 3.99$ Å), or Be ($\lambda > 3.99$ Å) filter (component 1 in Fig. 1), cooled to liquid nitrogen temperature is placed upstream of the PG monochromator (component 2 in Fig. 1). Using the (002) crystal plane reflection of a PG monochromator, λ 's of 2.37, 4.00, and 5.23 Å are obtained for monochromator angles (θ_M) of 20.69°, 36.5°, and 51.25°, respectively. The PG monochromator used was of dimensions 5 cm(height) \times 8.9 cm(wide) \times 0.16 cm(thick).

Selected neutrons then go through a 66 cm long (the length denoted as L_{CSC}) CSC (component 3 in Figs. 1 and 2) made up of 23 channels, whereby each channel is separated by 0.25 mm spring steel blades coated with Gd_2O_3 . All chan-

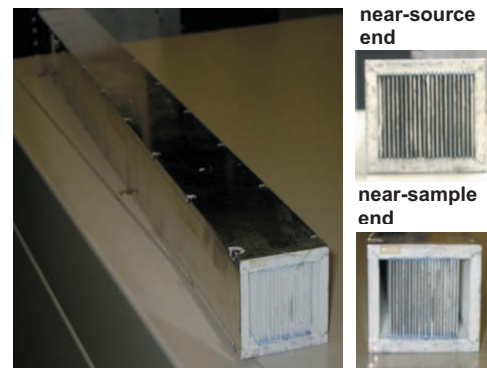


FIG. 2. (Color) Photograph of the 23-channel CSC.

nels converge on the same spot at the detector. Each individual channel has dimensions of 3.8 cm (high) by 0.13 cm (wide) at the monochromator end and 3.8 cm (high) by 0.10 cm at the end closest to the sample. The nearest distance from the monochromator to the CSC, D_{MC} , is 15 cm. For $\lambda = 4$ and 2.37 Å neutrons, the width of each channel can be increased to twice the original width by removing alternating Sollers.

After exiting the CSC, neutrons go through component 4 (Fig. 1), which for 2.37 Å neutrons is a PG filter, or in the case of 5.23 Å neutrons, a 21.6 cm long HSC with 0.25 cm vertical opening individual channels. In the case of 4 Å neutrons, component 4 is removed. At this point, the correct wavelength neutrons interact with the sample (component 5 in Fig. 1), located 86 cm from the nearest point to the CSC (denoted as D_{CS}). The scattered neutrons then go through a 48 cm long HSC containing 0.25 cm high individual channel (component 6 in Fig. 1). A 32-wire 3He position-sensitive detector (component 7 in Fig. 1) is placed after the second HSC with an effective sample-to-detector distance, D_{SD} , of 1.43 m. Each wire is capable of detecting scattered neutrons at the corresponding θ . Prior to experimentation, the efficiency of each detector wire was determined, and was later used to correct the data.

III. DATA REDUCTION

Scattered intensity, $I_{raw}(q)$, can be obtained from the following equation:

$$I_{raw}(q) = I_o \Delta\Omega \eta T_{sam}(\lambda) V \frac{d\Sigma}{d\Omega}(q) + I_{bgd}(q), \quad (1)$$

where I_o , $\Delta\Omega$, η , $T_{sam}(\lambda)$, V , and $I_{bgd}(q)$ are incident neutron intensity, sample-to-detector solid angle, detector efficiency, transmission of the sample, scattering volume, and background. $(d\Sigma/d\Omega)(q)$ represents the differential scattering cross section per unit volume and contains all of the pertinent sample information (e.g., shape, interactions, etc.). The goal of a SANS experiment is to obtain $(d\Sigma/d\Omega)$ as a function of q , which is used to determine the morphology of a given system. Therefore, appropriate data reduction has to be performed in order to obtain $(d\Sigma/d\Omega)(q)$ from the measured scattered intensities.

In our experiment, $I_{\text{raw}}(q)$ are collected using different wavelength neutrons ($\lambda=2.37, 4,$ and 5.23 \AA) and several detector angles in order to cover the desired q range. The data are normalized by incident neutron flux monitored using a low-efficiency neutron detector located after the CSC. The normalized scattered intensity of the empty cell, $I_{\text{emt}}(q)$ and $I_{\text{bgd}}(q)$ are obtained at the same q values. The reduced intensity, $I_{\text{red}}(q)$, can then be expressed as follows:

$$I_{\text{red}}(q) = \frac{[I_{\text{raw}}(q) - I_{\text{bgd}}(q)]}{T_{\text{sam}}(\lambda)} - \frac{[I_{\text{emp}}(q) - I_{\text{bgd}}(q)]}{T_{\text{emp}}(\lambda)}. \quad (2)$$

The sample and empty cell transmissions, $T_{\text{sam}}(\lambda)$ and $T_{\text{emp}}(\lambda)$, respectively, are determined from the straight through beam intensity (measured by the two central detector wires at $\theta=0^\circ$) ratios of the sample-to-open beam and the empty cell-to-open beam. $I_{\text{red}}(q)$ is then put on an absolute scale using a sample with a known $(d\Sigma/d\Omega)(q)$. Finally, the reduced intensities for the various q ranges are merged, yielding a single SANS curve.

IV. RESULTS AND DISCUSSION

A. Characterizing the Incident Beam from CSC

The CSC was tested prior to performing SANS measurements. In order to verify the point of beam convergence, the incident beam profiles on the detector at various locations of the CSC along the beam direction axis were measured [shown in Fig. 3(a)]. The data show the optimal D_{MC} —the distance resulting in the highest incident intensity at $\theta=0^\circ$ and the narrowest beam width at the detector—to be $\sim 15 \text{ cm}$, a value consistent with the specified collimator design. Each channel was also scanned with a 0.1 cm slit (slit width is equal to the width of a single CSC channel) across the CSC. Figure 3(b) shows the incident intensity of individual channels, whose intensities remain practically unchanged up to channel 14. The decrease in the neutron flux from channel 15 on, is most likely due to an insufficient monochromator size and/or displacement of the monochromator (no translational capability). Figure 3(c) shows a comparison of the total intensity (all channels opened) with that from individual channels. A Lucite absorber was used for the measurements with all the channels open to avoid saturating the detector. The data shown in Figure 3(c) were corrected by the Lucite's absorption factor. The neutron beams from individual channels of size $3.8 \times 0.1 \text{ cm}^2$ project onto the detector at proximate locations. When fitted with a Gaussian function, the centers of the peak positions vary within $\pm 0.03^\circ$ from each other, which translates into $\pm 6.3 \times 10^{-4} \text{ \AA}^{-1}$ for $\lambda=5.23 \text{ \AA}$ (low q) and $\pm 1.4 \times 10^{-3} \text{ \AA}^{-1}$ for $\lambda=2.37 \text{ \AA}$ (high q) in Δq . These values are at least an order of magnitude lower than the calculated resolution functions in shown in Sec. IV B, and do not affect the accuracy of the data. The increased background-to-direct beam ratio and the broad peaks on both sides of the beam when all channels are opened, are presumably the result of low- q scattering from the Lucite attenuator. It is clear that the CSC enhances the incident neutron intensity by a factor of 20, compared to that

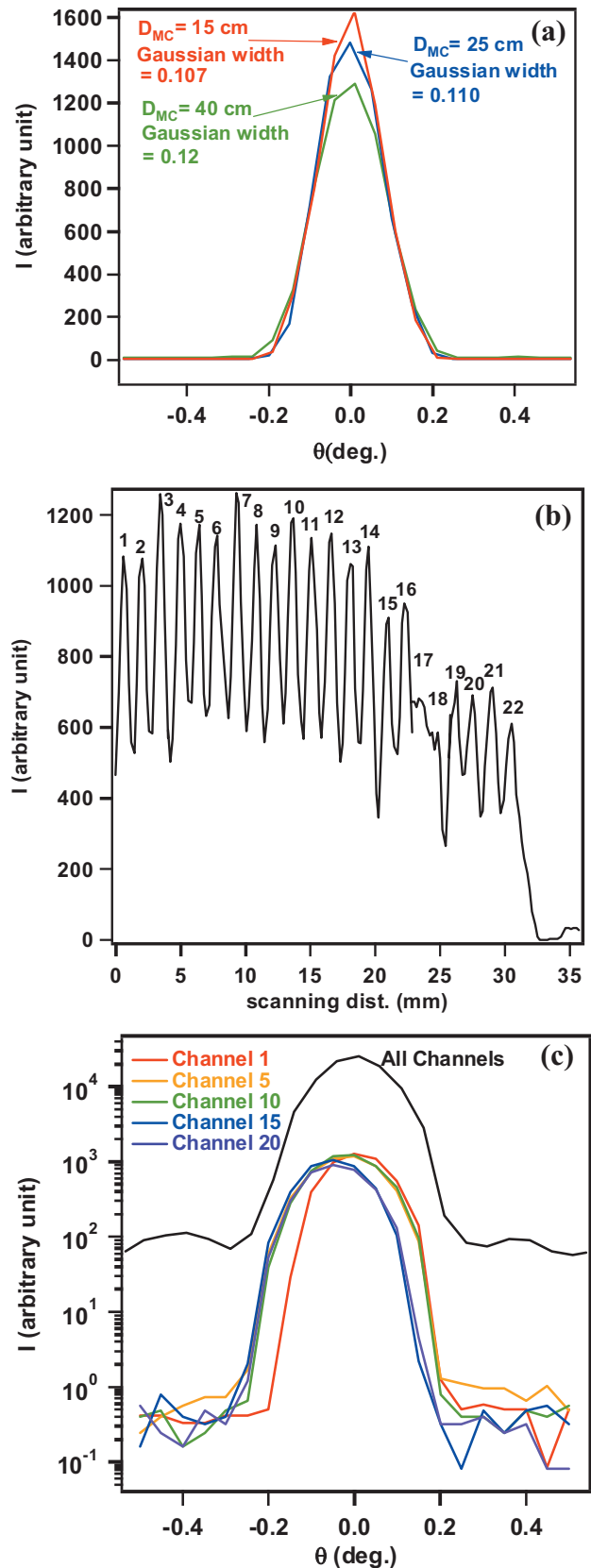


FIG. 3. (Color) (a) Characterization of the incident beam width (all channel open) at various D_{MC} . (b) Characterization of the individual CSC channels. (c) Comparison of the incident beam intensity from individual channels (1, 5, 10, 15, 20) and all channels.

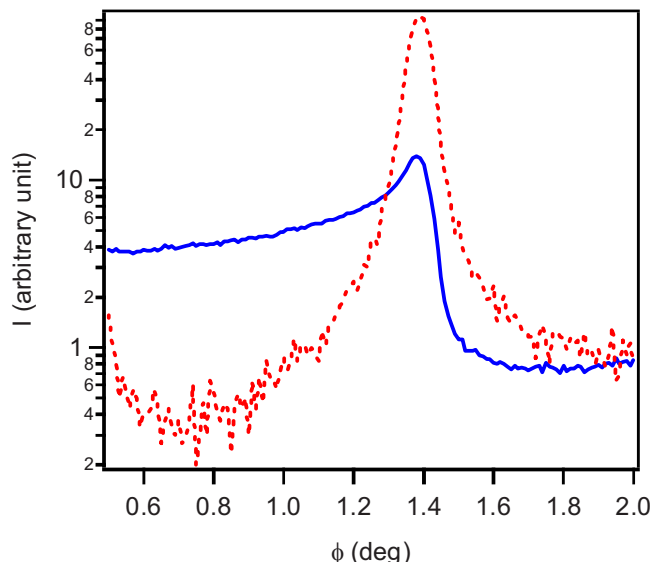


FIG. 4. (Color online) SAXS data of a DMPC sample with (dotted curve) and without (solid curve) a 0.5° divergence HSC after the sample.

from each individual channel, without any noticeable effect on the projected beam size (at the detector). Ideally, using a curved monochromator the expected increase in intensity would be 23 times, equal to the number of CSC channels.

B. The resolution function

A SANS instrument's resolution function depends on the collimation used (e.g., pinhole, slit, etc.). In a slit geometry where the x and y dimensions of the slit differ considerably, there is a significant difference between the q variances of the two orthogonal components in the detector plane (q_x - q_y), $\sigma_{q_x}^2$ along the θ direction and $\sigma_{q_y}^2$ in the orthogonal direction, resulting in an asymmetric smearing of the data, (i.e., when $\sigma_{q_y}^2 \gg \sigma_{q_x}^2$). This effect is demonstrated in Fig. 4, which shows a small angle x-ray scattering (SAXS) result from a 1% phospholipid dispersion [dimyristoyl phosphatidylcholine (DMPC) in water] obtained using an Ultima III diffractometer (Rigaku, Japan). The x-ray diffractometer, with a line source of x-rays, was set up with a 0.5° divergence HSC on the incident side. The two curves show SAXS data with and without a 0.5° divergence HSC on the detector side. A peak (obtained with the HSC on the detector side) corresponding to the lamellar spacing of DMPC is not only smeared, but is also asymmetric in the absence of the HSC on the detector side. Generally, the magnitudes of $\sigma_{q_x}^2$ and $\sigma_{q_y}^2$ for a slit geometry can be expressed as

$$\sigma_{q_x}^2 = \left(\frac{\pi^2}{6\lambda^2} \right) \left[\frac{X_1^2(D_{CS} + D_{SD})^2}{L_{CSC}^2 D_{SD}^2} + \frac{X_2^2(L_{CSC} + D_{CS} + D_{SD})^2}{L_{CSC}^2 D_{SD}^2} + \left(\frac{X_3}{D_{SD}} \right)^2 + \left(\frac{q_x}{q} \right)^2 \theta^2 \left(\frac{\Delta\lambda}{\lambda} \right)^2 \right],$$

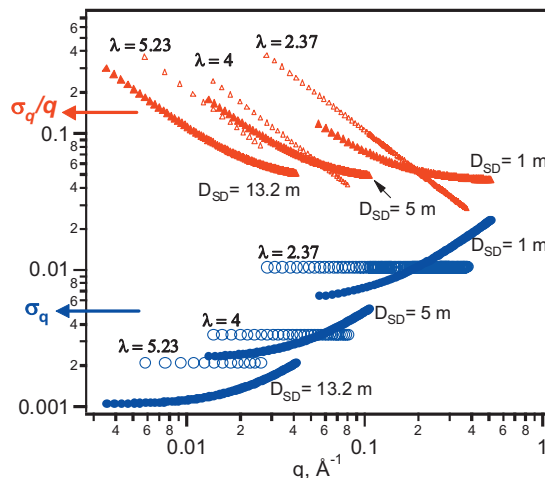


FIG. 5. (Color) Instrumental resolution of the N5- and NG3-SANS instruments. Both $\sqrt{\sigma_{q_x}^2}/q$ (red triangles) and $\sqrt{\sigma_{q_y}^2}$ (blue circles) are plotted as a function of q . Hollow and solid symbols represent N5-SANS and NG3-SANS data, respectively.

$$\sigma_{q_y}^2 = \left(\frac{\pi^2}{6\lambda^2} \right) \left[\frac{Y_1^2(D_{CS} + D_{SD})^2}{L_{CSC}^2 D_{SD}^2} + \frac{Y_2^2(L_{CSC} + D_{CS} + D_{SD})^2}{L_{CSC}^2 D_{SD}^2} + \left(\frac{Y_3}{D_{SD}} \right)^2 + \left(\frac{q_y}{q} \right)^2 \theta^2 \left(\frac{\Delta\lambda}{\lambda} \right)^2 \right],$$

$$\sigma_q^2 = \sigma_{q_x}^2 + \sigma_{q_y}^2, \quad (3)$$

where (X_1, Y_1) , (X_2, Y_2) , and (X_3, Y_3) are slits for the beam source, the sample, and the detector along q_x and q_y , respectively.^{1,2}

To minimize peak asymmetry, as shown in Fig. 4, the dimension of $\sigma_{q_y}^2$ should approach that of $\sigma_{q_x}^2$. However, since X_1 , X_2 , and X_3 are highly constrained by the CSC and the width of the individual detector wires (~ 2 mm), $\sigma_{q_y}^2$ is relaxed, compared to $\sigma_{q_x}^2$ (still maintaining a slit geometry), allowing for a sufficient neutron flux. This way, $\sigma_{q_y}^2$ dominates σ_q^2 . Figure 5 shows a plot of σ_q/q and σ_q ($\sigma_q = \sqrt{\sigma_q^2}$) as a function of q . As expected from Eq. (2), for a given λ , σ_q remains almost constant, and most of the smearing (i.e., σ_q/q) takes place at the lowest θ s. Figure 5 also shows a comparison of this result with that from a pinhole geometry instrument (NG3-SANS) located at the NIST Center for Neutron Research.¹⁶ The resolution function of the NG3-SANS is calculated based on a neutron wavelength of 6 \AA , a $\Delta\lambda/\lambda$ of 15% and three D'_{SD} s (1, 5 and 13.2 m). The magnitude of σ_q (Fig. 5) increases at higher q values as a result of the poor wavelength resolution ($\Delta\lambda/\lambda \sim 15\%$ in this case), and eventually becomes comparable to the first three terms [in Eq. (2)] related to distance collimation. However, this increase in σ_q does not worsen the smearing effect (comparing to lower q values), as σ_q/q continues to decrease with increasing q . At low q the instrumental resolution, σ_q/q of the N5-SANS is worse than the NG3-SANS at $q < 0.05 \text{ \AA}^{-1}$, but comparable and sometimes even better at $q > 0.1 \text{ \AA}^{-1}$.

For N5-SANS, the apparent q values, q_{app} are obtained from $(4\pi/\lambda)\sin(\theta_{app}/2)$, where θ_{app} is $\tan^{-1}(R/D_{SD})$, and

where R is the distance from the center of the individual detecting wires to the center of the incident beam in the scattering plane. The mean q value, q' , is thus different from q_{app} and can be derived based on the two components of the resolution function (σ_{q_x} and σ_{q_y}). We assume a 2D Gaussian distribution of the contributed intensity from various qs (on the q_x - q_y plane) centered at q_{app} . Since the scattered intensity along the q_y axis is symmetric around the horizontal center line ($q_y=0$) of the detector [i.e., $I_{\text{raw}}(q_x, q_y) = I_{\text{raw}}(q_x, -q_y)$], but not symmetric along the q_x axis around the vertical center line ($q_x=0$) [i.e., $I_{\text{raw}}(q_x, q_y) \neq I_{\text{raw}}(-q_x, q_y)$], different integration boundaries are applied to q_x and q_y [i.e., $(-\Delta q_{x,\text{max}}, \Delta q_{x,\text{max}})$ for q_x and $(0, \Delta q_{y,\text{max}})$ for q_y , where $\Delta q_{x,\text{max}}$ and $\Delta q_{y,\text{max}}$ are calculated from the maximal divergence in the frame of scattering geometry]. Since the values of $\Delta q_{x,\text{max}}$ and $\Delta q_{y,\text{max}}$ are more than seven times of σ_{q_x} and σ_{q_y} under all circumstances, the integration of Gaussian function covers more than 99.9% of that over infinity. As a result, an analytic solution $q' = \sqrt{q_{\text{app}}^2 + \sigma_{q_y}^2} / \pi$ can be written as follows:

$$q'^2 = q_x'^2 + q_y'^2,$$

$$q_x' = \frac{\int_{-\infty}^{\infty} q_x e^{-\frac{(q_x - q_{\text{app}})^2}{\sigma_{q_x}^2}} dq_x}{\int_{-\infty}^{\infty} e^{-\frac{(q_x - q_{\text{app}})^2}{\sigma_{q_x}^2}} dq_x}$$

and

$$q_y' = \frac{\int_0^{\infty} q_y e^{-\frac{(q_y - q_{\text{app}})^2}{\sigma_{q_y}^2}} dq_y}{\int_0^{\infty} e^{-\frac{(q_y - q_{\text{app}})^2}{\sigma_{q_y}^2}} dq_y}. \quad (4)$$

C. Experimental results

Using the N5-SANS, we examine two standard polystyrene microsphere samples with diameters of 24 and 50 nm (PS02N, Bangs Laboratories). The microspheres arrived as 10 wt % solutions and were subsequently diluted to 1 wt % with D_2O (Atomic Energy of Canada Limited, Chalk River, Ontario, Canada). The samples were loaded in rectangular quartz cells having a 5 mm path length. The absolute intensities (i.e., $d\Sigma/d\Omega$) for both samples are obtained from the NG3-SANS, as shown in Figs. 6(a) and 6(c). To obtain the best-fit structural parameters, NG3-SANS data are fitted using a core-shell-sphere model convoluted with the instrumental resolution. The same model and structural parameters are used to rescale the scattering data of the samples obtained from N5-SANS; however, this time taking into consideration the N5-SANS instrumental resolution [Figs. 6(b) and 6(d)]. The N5-SANS data are rescaled for each q range and then plotted on the same figure. Slight discontinuities at the overlapping regions of the rescaled data are observed, presumably due to different resolution functions of the individual q ranges. We find good agreement between NG3-SANS and N5-SANS data [Figs. 6(b) and 6(d)] (slight discrepancies in

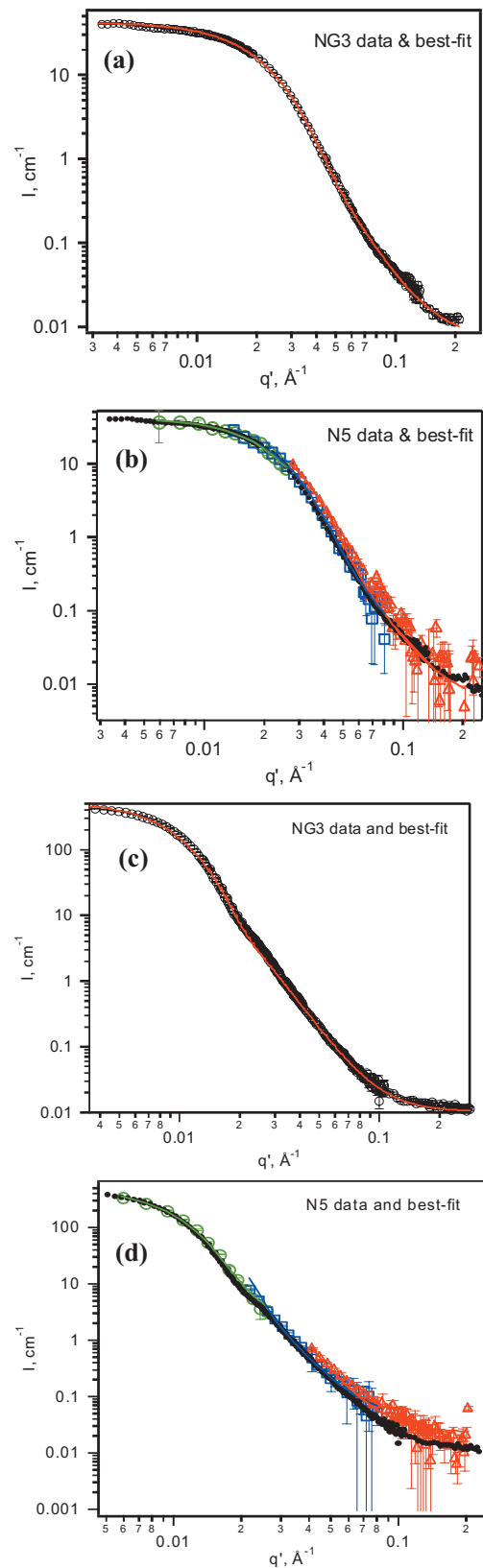


FIG. 6. (Color) SANS data of 1 wt % microspheres with a diameter of 24 nm obtained from (a) the NG3-SANS and (b) the N5-SANS, and 1 wt % 50 nm diameter microspheres from (c) the NG3-SANS and (d) the N5-SANS. The best fits using a core-shell-sphere model are shown as solid lines. N5-SANS data are rescaled using the same model and structural parameters as the NG3-SANS, but different instrumental resolution. Circles, squares, and triangles in (b) and (d) represent the SANS configurations using $\lambda = 5.23, 4,$ and 2.37 \AA , respectively. NG3-SANS data (dots) are also plotted in (b) and (d) for comparison purpose.

slopes of the two curves are the result of different resolution functions and incoherent background subtraction) proving the successful implementation of this SANS design. The total data collection time at the N5-SANS was ~ 4.5 h ($1\frac{1}{2}$ h for $\lambda=5.23$ Å, 1 h for $\lambda=4$ Å, and 1 h for $\lambda=2.37$ Å), compared to 40 min at the NG3-SANS. Moreover, the counting statistics of the N5-SANS data are poorer than those obtained at the NG3-SANS data. The reasons for this are twofold: (1) the small detecting area of the 32-wire N5-SANS detector (12×6.5 cm²) requires multiple detector locations to cover a given q range (compared to the much larger 65×65 cm² 2D detector at NG3). (2) For weakly scattering samples, air scattering dominates at low q , thus longer collecting times are needed to reduce the errors when subtracting the air scattering from the sample scattering. This latter issue is presently being addressed through the use of evacuated HSCs.

V. CONCLUSIONS

We have reported on adapting a triple-axis spectrometer for use in SANS measurements. Data (from 0.006 to 0.3 Å⁻¹) obtained from such an instrument (i.e., N5-SANS) agree well with those collected from the well-established 30 m NG3-SANS. Compared to the NG3-SANS, the instrumental resolution is poorer at low q ($q < 0.05$ Å⁻¹), but comparable, or even better, at high q ($q > 0.1$ Å⁻¹). Although the measurements at the N5-SANS compared to the NG3-SANS take longer, this situation can, to some extent, be remedied through the use of evacuated HSCs, which are currently under construction.

ACKNOWLEDGMENTS

This work utilized facilities supported in part by the National Science Foundation under Agreement No. DMR-9986442. M.-P. N. would like to thank Dr. John Barker, Dr. Charles Glinka, and Dr. Boualem Hammouda (NIST) for the helpful discussions.

- ¹S. M. Choi, J. G. Barker, C. J. Glinka, Y. T. Cheng, and P. L. Gammel, *J. Appl. Crystallogr.* **33**, 793 (2000).
- ²D. F. R. Mildner and J. M. Carpenter, *J. Appl. Crystallogr.* **17**, 249 (1984).
- ³D. F. R. Mildner and J. M. Carpenter, *J. Appl. Crystallogr.* **20**, 419 (1987).
- ⁴H. R. Child and S. Spooner, *J. Appl. Crystallogr.* **13**, 259 (1980).
- ⁵D. F. R. Mildner, R. Berliner, O. A. Pringle, and J. S. King, *J. Appl. Crystallogr.* **14**, 370 (1981).
- ⁶B. J. Heuser, M. Popovichi, W. B. Yelon, and R. Berliner, *Proc. SPIE* **1738**, 210 (1992).
- ⁷V. K. Aswal and P. S. Goyal, *Curr. Sci.* **79**, 947 (2000).
- ⁸V. K. Aswal, J. V. Joshi, P. S. Goyal, and A. V. Pimpale, *J. Appl. Crystallogr.* **33**, 118 (2000).
- ⁹A. C. Nunes, *Nucl. Instrum. Methods* **119**, 291 (1974).
- ¹⁰C. J. Glinka, J. M. Rowe, and J. LARock, *J. Appl. Crystallogr.* **19**, 427 (1986).
- ¹¹U. Bonse and M. Hart, *Appl. Phys. Lett.* **7**, 238 (1965).
- ¹²U. Bonse and M. Hart, *Z. Phys.* **189**, 151 (1966).
- ¹³A. R. Drews, J. G. Barker, C. J. Glinka, and M. Agamalian, *Physica B (Amsterdam)* **241–243**, 189 (1998).
- ¹⁴F. U. Ahmed, I. Kamal, S. M. Yunus, T. K. Datta, A. K. Azad, A. K. M. Zakaria, and P. S. Goyal, *Physica B (Amsterdam)* **366**, 11 (2005).
- ¹⁵H. F. Nieman, D. C. Tennant, and G. Dolling, *Rev. Sci. Instrum.* **51**, 1299 (1980).
- ¹⁶C. J. Glinka, J. G. Barker, B. Hammouda, S. Krueger, J. J. Moyer, and W. J. Orts, *J. Appl. Crystallogr.* **31**, 430 (1998).